A Theoretical Study on the Third-Order Nonlinear Optical Properties of π-Conjugated Linear Porphyrin Arrays

Yoichi Matsuzaki*

Advanced Technology Research Laboratories, Nippon Steel Corporation, 20-1 Shintomi, Futtsu, Chiba 293-8511, Japan

Atsushi Nogami

Department of Environmental Space Design, The University of Kitakyushu, 1-1 Hibikino, Wakamatsu-ku, Kitakyushu, Fukuoka, 808-0135, Japan

Akihiko Tsuda and Atsuhiro Osuka

Department of Chemistry, Kyoto University, Kyoto 606-8502, Japan

Kazuyoshi Tanaka

Department of Molecular Engineering, Graduate School of Engineering, Kyoto University, Nishikyo-ku, Kyoto 615-8510, Japan

Received: November 30, 2005; In Final Form: January 26, 2006

By using the Pariser−Parr−Pople (PPP) theory, the second hyperpolarizabilities (γ) have been calculated for various π-conjugated porphyrin arrays including "porphyrin tapes": the *meso*-β doubly linked porphyrin array **D*n*** and the *meso*−*meso*, $\beta-\beta$, $\beta-\beta$ triply linked array **T*n***. The validity of the PPP theory is checked via a comparison with both the ab initio Hartree−Fock and the B3LYP theories in the case of porphyrin monomers and dimers. It is found that **D*n*** and especially **T*n*** exhibit much more remarkable evolution of γ/n along with an increasing number of porphyrin units n compared with the butadiyne-bridged array, **Y*n***. As a result, the static third-order susceptibilities $\chi^{(3)}$ of **D*n*** and **T*n*** are expected to be 1 and 3 orders of magnitude larger than that of **Y*n*** in the limit $n \rightarrow \infty$, and these advantages of porphyrin tapes become more prominent by taking into account geometrical relaxations of porphyrin units in the arrays. The structure−property relationship in various conjugated polymers including porphyrin arrays is interpreted on the basis of the scaling behaviors of $\chi^{(1)}$ and $\chi^{(3)}$ with the effective conjugation length (ECL) as well as the reciprocal HOMO−LUMO energy gap ($1/E_g$). In particular, from the master plot of $\chi^{(3)}$ (and even $\chi^{(1)}$) versus $1/E_g$, the π-conjugation of **T*n*** is noted to indeed be exceptional, because its large susceptibilities cannot be expected from the scaling behavior of ordinary one-dimensional conjugated systems. We also point out that the theory of scaling relationship, $\chi^{(3)} \sim 1/E_g^x$, is significantly improved by taking into account electron−electron interactions based on the comparison with experiments.

I. Introduction

During the last two decades, there has been a great deal of interest in the nonlinear optical (NLO) responses of conjugated organic molecules and polymers both from a fundamental perspective and because of their potential utility in various photonic applications.[1−5] The real part of the third-order NLO susceptibility $\chi^{(3)}(-\omega; \omega, \omega, -\omega)$ gives rise to nonlinear refraction that can be utilized for all-optical signal processing,[6] while the imaginary part controls two-photon absorption (TPA) which is useful for many applications such as 3-D optical memory,[7] optical power limiting,[8] and photodynamic therapy.[9] To realize these applications, sufficiently large optical nonlinearity is essential, and especially for the former application, additional requirements should be fulfilled by the NLO material, i.e., fast response time and transparency at the operating wavelength window. The classical π-conjugated polymers such as polydiacetylene (**PDA**)[10] and poly(*p*-phenylene vinylene) (**PPV**, Figure 1)[11] exhibit fast NLO responses in the off-resonant condition; however, they do not offer sufficiently large nonlinearities. Then, suitable material has yet to be convincingly demonstrated as having the full range of required attributes.

In the search for improved NLO materials, porphyrins are promising candidates for building-block elements because of their large polarizable π systems. From this, it can be inferred that, by linking porphyrin molecules into oligomers, the extended movement of the π electrons into the neighboring moieties can further enhance their optical nonlinearities. Butadiyne-bridged porphyrin arrays (**Y*n***, Figure 1) exhibit efficient π-electron delocalization throughout the entire backbone as revealed by its progressively red-shifted Q-band absorption that reaches approximately 850 nm at $n = 10-15$.[12] It was found that the **Y*n*** polymer has the largest one-photon off-resonant $\chi^{(3)}$ reported for any organic material,[13] and an

* To whom correspondence should be addressed. E-mail: matuzaki@re.nsc.co.jp.

10.1021/jp0582989 CCC: $33.50
Published on Web 03/17/2006

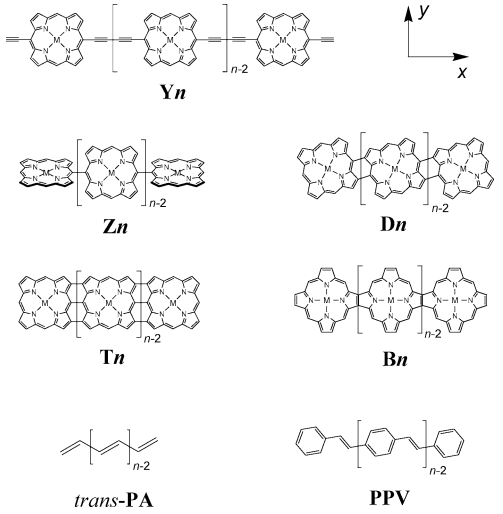

Figure 1. Chemical structure and axis definition for the porphyrin arrays and the classical π-conjugated polymers investigated in this work.

exceptionally large TPA cross-section ($\sigma^{(2)}$) was measured on the double-strand ladder complex of **Y*n***.[14]

On the other hand, directly linked porphyrin arrays have been developed starting from the *meso-meso* directly linked porphyrin arrays **Z*n*** (Figure 1).[15] Although the π-electron delocalization is disrupted in **Z*n*** because of the orthogonal arrangement of neighboring porphyrin units, they exhibit unique electrooptic responses at the Soret-band region as a result of the close proximity of adjacent macrocycles.[16] Through the efficient synthetic method, **Z*n*** have been successfully transformed into the *meso*−*meso*, $\beta-\beta$, $\beta-\beta$ triply linked "porphyrin tapes" (**T*n***, Figure 1).[17] The porphyrin tapes thus prepared are exceptional molecules, because their Q-band absorption becomes progressively red-shifted with an increase in the number of porphyrin moieties without indication of any saturation at least up to $n = 12$. As an extreme case, **T12** exhibits a very low optical gap that reaches approximately 2.8 μm. With these in the background, **T*n*** is intriguing in view of potential applications not only as moleular electric wire but also as NLO material. In fact, a remarkable NLO response of **T*n*** is currently being revealed, for instance, by the measurement of $\sigma^{(2)}$ on **T2**[18] and its derivative.[19] Furthermore, the *meso*-β doubly linked porphyrin tapes (**D*n***, Figure 1) have been successfully prepared up to $n = 5$ in the Ni^{II}-metalated form.[20] They also exhibit a progressive red-shift of the Q-band absorption with an increase in the number of porphyrin units, although it is not as remarkable as **T*n***. In addition, β-fused oligoporphyrins (**B*n***, Figure 1) have been reported up to the trimer.[21]

These porphyrin arrays constitute a new class of π-conjugated polymers that can exhibit favorable electrical and optical properties never accessible by classical conjugated polymers. In this paper, we investigate the relationship between the structure of multi-porphyrin arrays and their third-order NLO responses, so as to provide a platform for the further development of porphyrin-based macromolecules. In this course, we are concerned with the concept of effective conjugation length (ECL).[22] Because ECL is closely related to the extent of π-electron delocalization, it must be a crucial quantity that determines the magnitude of $\chi^{(3)}$ of π-conjugated polymers.

The universal scaling between $\chi^{(3)}$ and ECL has been derived by Flytzanis and co-workers using the Hückel theory.[23−25] On the basis of the simple bond-length alternated chain, they introduced the delocalization length L_d that can be regarded as a measure of ECL and obtained the scaling laws for $\chi^{(3)}$ as well as linear susceptibility $\chi^{(1)}$

$$\chi^{(1)} \sim {L_d}^2 \tag{1}$$

$$\chi^{(3)} \sim {L_d}^6 \tag{2}$$

Since within the Hückel theory, L_d is inversely proportional to energy gap E_g between the highest occupied molecular orbital (HOMO) and the lowest unoccupied molecular orbital (LUMO), these equations have been cast into

$$\chi^{(1)} \sim 1/{E_g}^2 \tag{3}$$

$$\chi^{(3)} \sim 1/{E_g}^6 \tag{4}$$

that are more directly accessible to measurement if an optical gap is adopted as E_g. Although several experiments have proven the existence of such a scaling law for $\chi^{(3)}$, they also found significant deviations from eq 4, particularly, much larger exponents ($\sim$10)[26,27] than the theoretical value. Therefore, eqs 1−4 will be reinvestigated in this study, taking into account electron−electron interactions within the framework of the Pariser−Parr−Pople (PPP) theory.[28,29] Moreover, these scaling behaviors will be utilized to characterize the electronic structures of π-conjugated porphyrin arrays, pointing out an exceptional feature of **T*n***.

II. Computational Methods

In this study, we calculate the microscopic polarizabilities of a single molecular chain, because they are the essential quantities that determine the optical response of a bulk material. When static external electric field $\boldsymbol{F}$ is applied to a molecule, it induces a dipole moment

$$\Delta\mu(\boldsymbol{F}) = \alpha\boldsymbol{F} + \beta\boldsymbol{F}^2 + \gamma\boldsymbol{F}^3 + ... \tag{5}$$

where α, β, and γ are the linear polarizability, the first hyperpolarizability, and the second hyperpolarizability, respectively. γ is responsible for the third-order NLO response and is the quantity of major interest in this study. The α and γ values of the porphyrin arrays were calculated using the PPP method, because it can be applied to sufficiently long arrays (up to **T30** in this study) that are required to assess the saturation of γ per repeating units. The accuracy of the simple PPP method was checked via a comparison with the ab initio Hartree−Fock (HF) theory and the B3LYP hybrid density functional theory (DFT) in the case of porphyrin monomers and dimers. Unless otherwise mentioned, all of the ab initio HF and B3LYP calculations were conducted using the Gaussian 98 suite of programs.[30] Throughout this study, any substituents attached on the periphery of the porphyrin macrocycles were omitted, and the actual geometries of the investigated systems were determined as follows.

In the PPP calculations, the geometries of constituent porphyrin rings in the arrays were constrained to that of Zn^{II}-tetraphenylporphyrin (Zn^{II}-TPP) as revealed by X-ray crystallography.[31] For **T*n***, the subunits were arranged keeping a *meso-meso* bond length of 1.51 Å as found in the X-ray structure of Zn^{II}-**T2**,[17a] which leads to a $\beta-\beta$ distance of 1.455 Å being close to the experimental value of 1.44 Å. In the case of **D*n***, the subunits were arranged with a *meso*−β bond length of 1.45 Å as observed in the X-ray structure of Ni^{II}-**D2**.[20a] Although porphyrin macrocycles adopt a ruffled conformation in the X-ray structure of Ni^{II}-**D2**, we assumed a flat geometry for the sake

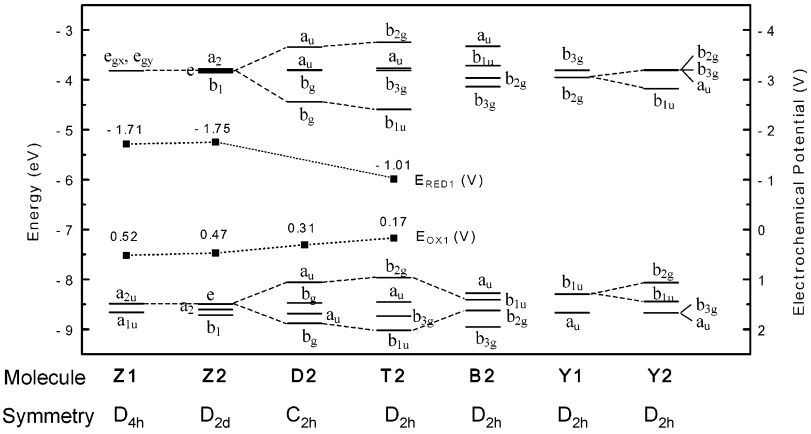

Figure 2. PPP-calculated energy level of the frontier orbitals of porphyrin monomers and dimers. The orbital interactions associated with the occupied a_{2u} (b_{1u}) and the unoccupied e_{gx} (b_{2g}) MOs of **Z1** (**Y1**) are indicated by the dashed lines. The experimental first oxidation potentials (E_{OX1}, ref 41) and reduction potentials (E_{RED1}, ref 42) are also plotted.

of simplicity. The geometries of **Y*n*** were constructed by adopting the X-ray bond lengths for the butadiyne linker of **Y2**:[32] 1.429, 1.210, and 1.368 Å for the C_{meso}—C, C≡C, and C—C bonds, respectively. Although the porphyrin macrocycles in the synthesized **B3** exhibit saddled conformations due to steric constraints from the periphery and/or core,[21] we assumed flat geometries for **B*n*** as an ideal case of this architecture. For classical conjugated polymers, *trans*-polyacetylene (*trans*-**PA**, Figure 1) and **PPV**, the bond lengths were fixed to be 1.45, 1.35, and 1.4 Å, for the single, double, and aromatic C—C bonds, respectively, and all the bond angles were set to 120°.

"Traditional" PPP parametrization[33] was employed, where the central metal ions were treated in an implicit manner and the first-neighbor transfer integrals were evaluated on the basis of the assumed geometries except for the $\beta-\beta$ linkages of **T*n***, which were based on the experimental bond length of 1.44 Å. For **Z2**, the inter-subunit transfer integrals at the $\alpha-\alpha$, $\beta-\beta$, and $\alpha-\beta$ carbon pairs (ca. 0.05 eV) were also taken into account. The intersite Coulomb interactions were evaluated using the Nishimoto−Mataga formula.[34] All of the PPP calculations of static α and γ were conducted using the coupled perturbed Hartree−Fock (CPHF) scheme.[35] In these calculations, the number of repeating units n in the oligomers was successively increased up to $n = 30$ for **T*n***, 20 for **D*n*** and **B*n***, 17 for **Y*n***, 70 for *trans*-**PA**, and 26 for **PPV**, while only the dimer was investigated for **Z*n*** because of the essentially disrupted interporphyrinic π-conjugation in this case.

The ab initio HF and B3LYP calculations of α and γ were conducted on a Zn^{II}-metalated series of porphyrin monomers and dimers, because this metalation has been reported for all the diporphyrins except **B2**. The geometries of these systems were optimized using the B3LYP method with the 6-31G* basis set[36,37] for carbon, nitrogen, and hydrogen and the [53321/5311/41] set for Zn.[38] The geometry optimization was performed under the highest possible symmetry constraints (D_{4h} for **Z1**, D_{2h} for **Y1**, **Y2**, **T2**, and **B2**, and D_{2d} for **Z2**) and has been confirmed to gain the minimum-energy structures by performing normal vibrational-mode analysis. We found both C_2 and C_i symmetry conformers for **D2**, with the former being more stable by 2 kcal/mol. Although this conflicts with the near C_i symmetry of the X-ray structure of Ni^{II}-**D2**,[20a] we found that these conformers have essentially the same α and γ values, and hence, only the results on the C_2 conformer will be reported.

The HF/6-31G* calculations of α and γ for monomeric porphyrins were performed using the CPHF method as implemented in the GAMESS code,[39] while the other ab initio HF and all of the B3LYP calculations were conducted using the finite-field (FF) method. In the FF scheme, the tensor components of α and γ were obtained by the numerical differentiations of total energy E with respect to the applied electric field

$$\alpha_{ii} = [30E(0) - 16\{E(F_i) + E(-F_i)\} + \{E(2F_i) + E(-2F_i)\}]/12F_i^2 \quad (6)$$

$$\gamma_{iiii} = -[56E(0) - 39\{E(F_i) + E(-F_i)\} + 12\{E(2F_i) + E(-2F_i)\} - \{E(3F_i) + E(-3F_i)\}]/36F_i^4 \quad (7)$$

$$\gamma_{iijj} = -[72E(0) - 38\{E(F_i) + E(-F_i) + E(F_j) + E(-F_j)\} + 2\{E(2F_i) + E(-2F_i) + E(2F_j) + E(-2F_j)\} + 20\{E(F_i, F_j) + E(F_i, -F_j) + E(-F_i, F_j) + E(-F_i, -F_j)\} - \{E(2F_i, F_j) + E(2F_i, -F_j) + E(-2F_i, F_j) + E(-2F_i, -F_j) + E(F_i, 2F_j) + E(F_i, -2F_j) + E(-F_i, 2F_j) + E(-F_i, -2F_j)\}]/72F_i^2F_j^2 \quad (8)$$

where $E(F_i)$ represents the total energy in the presence of static electric field F applied in the i ($= x, y, z$) direction. To obtain numerically stable γ values, the field strength was optimized to each system in the range of 0.0005 and 0.002 au, and the numerical accuracy of the B3LYP calculations was improved by using 99 radial and 590 angular points as an integration grid. For a comparison with experiments, the orientationally averaged α and γ values were evaluated as

$$\alpha_s = (\alpha_{xx} + \alpha_{yy} + \alpha_{zz})/3 \quad (9)$$

$$\gamma_s = (\gamma_{xxxx} + \gamma_{yyyy} + \gamma_{zzzz} + 2\gamma_{xxyy} + 2\gamma_{xxzz} + 2\gamma_{yyzz})/5 \quad (10)$$

III. Results and Discussion

One-Electron Structure of Porphyrin Dimers. Figure 2 shows the energy-level diagram for the eight frontier (the highest four occupied and the lowest four unoccupied) orbitals of porphyrin dimers as well as those for the Gauterman's four orbitals[40] of their constituent monomers as obtained by the PPP calculations. In addition, schematic illustrations of the frontier orbitals of these compounds are given in Figure 3. As can be seen from Figures 2 and 3, the eight orbitals are formed by the combinations of the monomers' four orbitals, and their energy shifts relative to the corresponding monomer levels are consistent with their bonding and antibonding natures at the intersubunit linkages. These energy shifts, and hence the energy

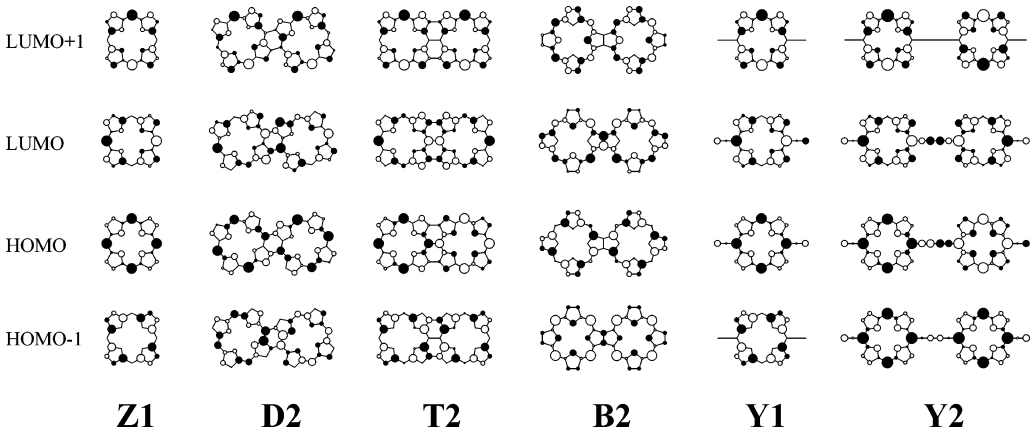

Figure 3. Schematic representation of the frontier orbitals of monomeric and dimeric porphyrins.

splitting among the eight orbitals, are more significant for the directly linked diporphyrins (**D2** and **T2**) than the butadiyne-bridged dimer (**Y2**), implying much more extensive π-conjugation in the former. The eight orbitals of **B2** are also regarded as a combination of the monomers' four orbitals, while the interaction of the constituent a_{1u} orbital is more significant than that of the a_{2u} orbital in contrast to the cases of **Y2** and **T2**.

The first oxidation (E_{OX1})[41] and reduction (E_{RED1})[42] potentials measured on the *meso*-aryl-substituted Zn^{II}-porphyrin compounds are also plotted in Figure 2 for comparison with the calculated HOMO and LUMO energies whose sign-reversed values represent ionization potential (IP) and electron affinity (EA), respectively, according to the Koopmans' theorem. As can be seen, the calculation is consistent with the experiment regarding the magnitude of electrochemical-potential shift for diporphyrins relative to **Z1,** which is expressed as **Z2** < **D2** < **T2**. Specifically, the most remarkable effect of dimerization is observed in the E_{RED1} of **T2**, which can be ascribed to the nature of its LUMO that exhibits constructive in-phase interaction at all three linkages.[43−45] Successful applications of π-electron PPP theory support the idea that the electrochemical properties of these Zn^{II}-diporphyrins are inherent in their π-electrons, and this would also be the case for other metalated series (Cu^{II}, Ni^{II}, Pd^{II}), because they also exhibit a similar dependence of E_{OX1} on the structure of the π-conjugated framework.[41]

At this stage, we should bear in mind the quasi-degeneracy of the a_{1u} and a_{2u} MOs of porphyrin, because the relative location of these MOs is responsible for the precise assignment of the first oxidized states of diporphyrins (**D2**, **T2**, and **B2**). The situation in the monomeric porphyrin is affected by both peripheral substitutions and central metal ions: *meso*-aryl groups preferentially raise the a_{2u} level, and the Zn^{II} ion prefers a_{2u} to be located above a_{1u} in comparison with other metal ions such as Cu^{II}, Ni^{II}, and Pd^{II}.[46,47] Then, the first oxidized state of **Z1** is most likely attributed to the $^2A_{2u}$ state, and accordingly, that of **T2** should be the $^2B_{2g}$ state (note that for the adiabatic ionization of **Z1**, a pseudo-Jahn−Teller distortion should also be taken into account[47]). We note that these experimental situations are well-reproduced by the present calculations despite the lack of *meso*-aryl groups and the implicit treatment of central metal ions. Therefore, the present PPP parametrization is also suited for a description of the longer **T*n***[17b] and **Y*n***[48,14] arrays, which have been prepared in a fashion similar to the diporphyrins; i.e., *meso*-aryl substitutions and Zn^{II} metalations.

One-Electron Structure of Porphyrin Arrays. In Figure 4, the energy levels of the HOMO and LUMO of the porphyrin arrays calculated using the PPP method are plotted against $1/L_x$, where L_x stands for the length of the π-system measured along the *x*-axis (Figure 1) for the following terminal atoms: the *meso* carbons for **D*n*** and **T*n***, the β carbons for **B*n***, and the alkyne carbons for **Y*n***. The orbital energies of infinitely long arrays were obtained using the crystal orbital method[49,50] adopting the same PPP Hamiltonian as the oligomers. As expected from the results on the dimers, both the HOMO and LUMO levels of **T*n*** (especially the latter) are remarkably shifted with an increase in the number of porphyrin units in the arrays:[44] the energy shifts from $n = 1$ to ∞ are 1.21 eV for the HOMO and 1.63 eV for the LUMO. To clarify the advantage of the triple linkage of **T*n***, we consider the hypothetical *meso*-*meso*-linked array **T*n*′** that is described by the same coplanar geometry and the PPP parameters as **T*n*** except the vanished transfer integrals for all the $\beta-\beta$ linkages. As seen in Figure 4, **T*n*′** exhibits a slightly

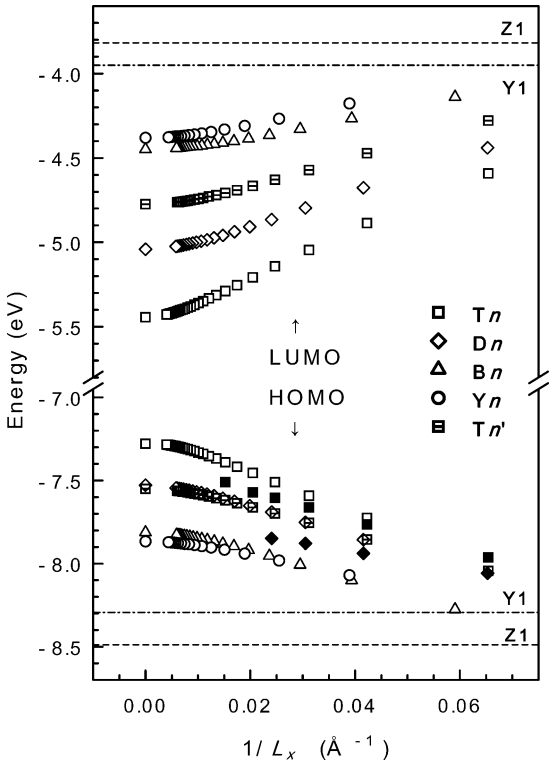

Figure 4. Plot of PPP-calculated HOMO and LUMO energies versus reciprocal chain length $1/L_x$ for π-conjugated porphyrin arrays, where the energies of infinite polymers were obtained by the crystal orbital method. The range of the number of repeating units *n* in the plot area is the same as in Figure 5. The energy levels of **Z1** and **Y1** are indicated by the horizontal lines. The filled symbols show the experimental first oxidation potentials of **T*n*** (ref 17b) and **D*n*** (ref 20b), which have been shifted to coincide with the theoretical HOMO energies at $n = 2$.

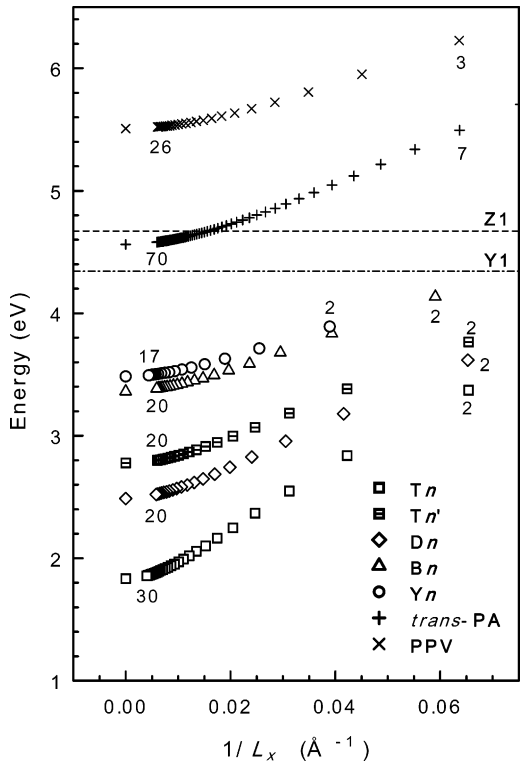

Figure 5. Plot of PPP-calculated HOMO−LUMO energy gap E_g versus reciprocal chain length $1/L_x$ for the π-conjugated porphyrin arrays, *trans*-**PA**, and **PPV**. The E_g values of **Z1** and **Y1** are indicated by the horizontal lines. The range of the number of repeating units n is also indicated.

pronounced shift of the frontier levels compared with **Y*n***, implying an advantage of the direct linkage over the butadiyne bridge for conjugation. From the comparison of **T*n*′** and **T*n***, it is evident that the additional $\beta-\beta$ linkages play a significant role in extending the π-conjugation especially for the LUMO.

The experimental first oxidation potentials (E_{OX1}) of **T*n***[17b] and **D*n***[20b] are also plotted in Figure 4. They indicate a more extensive π-conjugation for **T*n*** than for **D*n***: the E_{OX1} of the pentamer is reduced relative to that of the dimer by 0.36 V in **T*n*** and 0.21 V in **D*n***. Since the corresponding shifts of IP are calculated to be 0.45 and 0.37 eV, the calculation is qualitatively consistent with the experiment but overestimates the *n*-dependence of the energy shifts, especially for **D*n***. This discrepancy might be ascribed to the flat geometry of **D*n*** adopted in the PPP calculations ignoring the ruffling of macrocycles as observed in the X-ray structure of Ni^{II}-**D2**.[20a]

The data plot in Figure 4 is recast into that of HOMO−LUMO energy gap E_g in Figure 5. The reduction in E_g along with increasing array length becomes more significant as the number of interporphyrinic linkages is increased (**Y*n***, **T*n*′** < **D*n*** < **T*n***), and the remarkable feature of **T*n*** can be largely ascribed to the nature of its LUMO (Figure 4). As a result, the E_g of **T*n*** becomes much lower than those of the other porphyrin arrays. For comparison, we also investigated the representative π-conjugated polymers, *trans*-**PA** and **PPV**, adopting the same PPP parametrization as the porphyrin arrays. In Figure 5, it is noted that the E_g of both **D*n*** and **T*n*** exhibits much more retarded saturation than those of *trans*-**PA** and **PPV**, implying much greater ECL of these porphyrin arrays.

As seen in Figure 5, the theoretical E_g of **T*n*** does not indicate any saturation even at $n = 12$ (the longest array reported), in agreement with the experimental observations on the Q-band energy,[17b] while a precise comparison is not allowed because of the different natures of the relevant excited states (free electron−hole pairs in the former versus excitons in the latter). Moreover, the calculation predicts that the E_g of **T*n*** indeed saturates at a much longer array beyond $n = 12$; i.e., **T*n*** is not an intrinsic metal. In this regard, note that the calculated E_g values must be overestimated because of the lack of dynamical electron correlations at the HF level of theory, and including these effects, for instance, via the electronic polaron model, results in a significant reduction in E_g.[51] However, we believe our result is qualitatively correct, because there is no reason for **T*n*** polymer to have a partially filled energy band structure.

TABLE 1: Effective Conjugation Lengths (ECL) of π-Conjugated Polymers as Determined from the Saturation Behaviors of HOMO−LUMO Gap Energies (N_E) and Wavelengths (N_λ) and γ_{xxxx} Per Unit Segments (N_γ)

	N_E[a] (L_E)[b]		N_λ[c] (L_λ)		N_γ[d] (L_γ)
	0.14 eV	0.5 eV	10 nm	32 nm	
constrained geometric unit[e]					
Y*n*	5 (66.3)	2 (25.7)	5 (66.3)	3 (39.2)	2 (25.7)
T*n*	12 (99.2)	6 (48.9)	28 (233.6)	15 (124.4)	23 (191.6)
D*n*	9 (76.5)	4 (32.8)	16 (137.9)	8 (67.7)	7 (59.0)
T*n*′	8 (65.7)	4 (32.1)	13 (107.6)	7 (57.3)	6 (48.9)
B*n*	7 (59.3)	3 (25.4)	9 (76.2)	4 (33.9)	4 (33.9)
trans-**PA**	24 (56.9)	11 (25.4)	24 (56.9)	11 (25.4)	11 (25.4)
PPV	8 (48.1)	4 (22.2)	6 (35.2)	3 (15.7)	3 (15.7)
relaxed geometric unit[f]					
Y*n*	5 (66.3)	2 (25.7)	6 (79.8)	3 (39.2)	2 (25.7)
T*n*	15 (124.4)	7 (57.3)	≥25[g]	23 (191.6)	≥16[g]
D*n*	10 (85.2)	5 (41.5)	20 (172.5)	10 (85.2)	9 (76.5)
T*n*′	9 (74.1)	4 (32.1)	15 (124.4)	8 (65.7)	7 (57.3)
B*n*	7 (59.3)	3 (25.4)	9 (76.2)	5 (42.3)	4 (33.9)

[a] ECL determined by eq 11 with the thresholds ΔE_g of 0.14 and 0.5 eV. [b] The values in the parentheses are the corresponding oligomer lengths in Å units. [c] ECL determined by eq 12 with thresholds $\Delta\lambda_g$ of 10 and 32 nm. [d] For the explanation, see text. [e] The geometries of porphyrin units are constrained to the X-ray geometry of Zn^{II}-TPP. [f] The geometry relaxations of porphyrin units are taken into account as explained in the text. [g] Convergence could not be achieved in the calculations for $n \geq 25$ (SCF) and $n \geq 16$ (CPHF).

We determine the ECL of π-conjugated polymers on the basis of the criteria for the HOMO−LUMO energy gap

$$E_g(n) - E_g(\infty) \leq \Delta E_g \tag{11}$$

and the corresponding wavelength

$$\lambda_g(\infty) - \lambda_g(n) \leq \Delta\lambda_g \tag{12}$$

where $E_g(\infty)$ and $\lambda_g(\infty)$ are the limiting values for $n \rightarrow \infty$, and the smallest n values that fulfill eqs 11 and 12 are adopted as ECLs that will be referred to as N_E and N_λ, respectively. N_E reflects the saturation behaviors just as shown in Figure 5 and does not depend on the absolute value of E_g. On the other hand, because of the relationship $\lambda_g \sim 1/E_g$, the criterion of eq 12 leads to a greater ECL for the narrower gap systems; e.g., N_λ of a narrow gap system will be larger than that of a wide gap system even if they have same N_E.

As listed in Table 1, we applied these criteria to our computational results by setting ΔE_g to 0.14 and 0.5 eV and $\Delta\lambda_g$ to 10 and 32 nm. Although $\Delta\lambda$ was set to 1 nm in ref 52, which corresponds to the accuracy of an ordinary spectrometer, we adopt much larger values due to the initially small and progressively decreasing E_g of porphyrin arrays. Apparently, only a discussion on the relative value of ECL is meaningful, and it does not seem to be affected by the choice of ΔE_g and $\Delta\lambda_g$ values as seen in Table 1. To facilitate a comparison of ECL among different systems, the L_E and L_λ values (above-

TABLE 2: Poralizabilities α (in Å³) and Second Hyperpolarizabilities γ (in 10^{-36} esu) of Porphyrin Monomers and Dimers as Calculated Using the PPP, HF/6-31G*, and B3LYP/6-31G* Methods

	Z1	Z2	D2	T2	B2	Y1	Y2
				PPP			
α_{xx}	65.02	151.95	234.73	260.27	189.88	94.66	280.24
α_{yy}	65.02	65.01	121.73	121.04	120.73	65.19	127.45
α_{zz}	0	65.01	0	0	0	0	0
α_s	43.34	93.99	118.82	127.10	103.54	53.28	135.90
γ_{xxxx}	14.21	90.39	2734.57	2390.06	1599.49	164.19	7780.89
γ_{yyyy}	14.21	13.80	31.87	15.46	55.83	19.47	37.66
γ_{zzzz}	0	13.80	0	0	0	0	0
γ_{xxyy}	13.13	14.30	−11.17	31.89	−38.04	−9.09	−78.29
γ_{xxzz}	0	14.30	0	0	0	0	0
γ_{yyzz}	0	−0.00	0	0	0	0	0
γ_s	10.94	35.03	548.82	493.86	315.85	33.09	1532.40
γ_s ratio		0.07	1.1	1	0.64		3.1
E_g[a]	4.67	4.64	3.62	3.37	4.14	4.34	3.89
				HF/6-31G*			
α_{xx}	64.00	163.02	208.78	219.61	190.71	90.47	274.26
α_{yy}	64.00	73.13	114.86	116.82	117.21	66.68	129.24
α_{zz}	11.99	73.13	27.44	22.70	22.30	13.52	26.48
α_s	46.66	103.09	117.03	119.71	110.07	56.89	143.33
γ_{xxxx}	−12.12	68.48	904.59	556.95	972.47	37.35	2022.97
γ_{yyyy}	−12.12	5.21	−4.00	−21.07	21.49	−33.09	76.53
γ_{zzzz}	0.17	5.21	0.52	−2.03	0.44	0.16	2.82
γ_{xxyy}	15.16	44.24	−15.52	95.25	−100.92	8.17	−44.20
γ_{xxzz}	−0.02	44.24	−2.14	0.05	−0.26	0.10	2.42
γ_{yyzz}	−0.02	10.35	0.57	−0.03	0.05	−0.04	−4.10
γ_s	1.23	55.31	173.39	144.88	158.43	4.17	402.11
γ_s ratio		0.4	1.2	1	1.1		2.8
E_g	6.41	6.03	5.18	4.78	5.37	6.00	5.69
				B3LYP/6-31G*			
α_{xx}	65.18	170.74	231.57	244.53	192.99	97.70	359.53
α_{yy}	65.18	74.45	115.85	117.76	118.21	66.10	127.94
α_{zz}	12.28	74.45	28.03	23.21	22.85	13.80	27.01
α_s	47.55	106.55	125.15	128.49	111.35	59.20	171.49
γ_{xxxx}	2.61	250.69	873.38	527.10	852.41	42.05	9598.51
γ_{yyyy}	2.61	2.58	5.57	2.46	10.57	1.63	0.66
γ_{zzzz}	0.26	2.58	0.42	0.46	0.58	0.26	3.45
γ_{xxyy}	3.40	51.29	4.19	18.09	−7.40	−0.19	−35.86
γ_{xxzz}	0.03	51.29	0.33	0.16	0.23	0.10	1.11
γ_{yyzz}	0.03	0.09	0.45	−0.10	0.04	0.04	1.67
γ_s	2.48	92.23	177.86	113.26	169.86	8.77	1907.29
γ_s ratio		0.8	1.6	1	1.5		16.8
E_g	3.06	2.85	2.03	1.75	2.48	2.64	2.05

[a] HOMO−LUMO energy gap in eV.

mentioned L_x of the N_E- and N_λ-mers) are also given in Table 1. Because L_λ and even L_E of **PPV** are smaller than those of *trans*-**PA**, it is evident that the phenylene insertion is not favorable to extending π-conjugation. In contrast, these ECLs of **D*n***, **T*n***, and even **T*n′*** (constrained geometric unit models) are much larger than those of *trans*-**PA**, clearly demonstrating that the direct linkages of porphyrin units lead to quite extensive π-electron delocalization beyond the classical π-conjugated polymers.

Nonlinear Optical Properties of Porphyrin Dimers. Before applying the PPP theory to long porphyrin arrays, we check its accuracy via a comparison with the ab initio HF and the DFT theories as well as the available experimental data for porphyrin monomers and dimers. Although both the ab initio and DFT methods have been widely adopted in investigations of NLO responses of conjugated molecules and polymers, such studies on porphyrin compounds are limited.[53] Thus, we hope our study will also provide a platform for further theoretical studies on the NLO properties of various porphyrin-based macromolecules.

The α and γ values calculated by the PPP, HF/6-31G*, and B3LYP/6-31G* methods are summarized in Table 2. According to the DFWM (degenerate four-wave mixing) measurements at the 1064-nm wavelength,[48] the γ_s of **Y2** is increased by a factor of 76 relative to that of **Y1**, while this feature also owes to the much more significant two-photon resonance enhancement of γ in **Y2**. Therefore, the corresponding factor of 46 obtained using the PPP method would be reasonable, whereas that of 96 at the HF/6-31G* level is likely to be an overestimation. As listed in Table 3, we performed further calculations on the selected systems using the extended 6-31G*+p basis set, i.e., the 6-31G* set augmented with diffuse p-type functions on carbon ($\zeta_p = 0.0523$) and nitrogen ($\zeta_p = 0.0582$) atoms.[54] We found that these diffuse functions lead to a significant enhancement of γ_s for **Y1**, while their effects on **Y2** are almost negligible. This feature is consistent with the previous result that the influence of diffuse functions on the γ value becomes less significant with an increase in the chain length of polyenes.[55] As a result, the **Y2**/**Y1** γ_s ratio is reduced to 40 at the HF/6-31G*+p level, which is close to the PPP value. On the other hand, the static α_s of **Y2** is enhanced at most threefold relative to that of **Y1** at both PPP and ab initio HF levels, which is comparable to the experimental observation of sixfold enhancement in the Q-band oscillator strength.[48]

TABLE 3: Poralizabilities α (in Å³) and Second Hyperpolarizabilities γ (in 10^{-36} esu) of Z1, T2, Y1, and Y2 as Calculated with the Extended 6-31G*+p Basis Set at the HF and B3LYP Levels of Theory

	Z1	T2	Y1	Y2
		HF/6-31G*+p		
α_{xx}	68.10	231.66	96.18	287.34
α_{yy}	68.10	123.78	71.51	137.91
α_{zz}	19.37	35.18	21.52	41.70
α_s	51.85	130.21	63.07	155.65
γ_{xxxx}	−5.38	595.75	57.36	2257.27
γ_{yyyy}	−5.38	−15.17	−35.92	−62.38
γ_{zzzz}	1.93	3.08	1.99	4.71
γ_{xxyy}	20.53	101.57	11.06	−43.28
γ_{xxzz}	1.54	4.36	2.07	4.97
γ_{yyzz}	1.54	2.59	1.58	4.03
γ_s	7.68	160.14	10.57	426.21
		B3LYP/6-31G*+p		
α_{xx}	70.03	257.40	104.70	376.35
α_{yy}	70.03	125.80	71.34	137.45
α_{zz}	19.42	35.27	21.68	41.94
α_s	53.16	139.49	65.91	185.25
γ_{xxxx}	8.59	601.45	70.93	10611.26
γ_{yyyy}	8.59	12.35	7.14	14.63
γ_{zzzz}	2.13	3.52	2.25	4.60
γ_{xxyy}	6.27	25.59	2.25	−34.87
γ_{xxzz}	1.95	5.12	2.75	7.44
γ_{yyzz}	1.95	3.16	1.93	2.85
γ_s	7.93	137.01	18.83	2116.26

The γ values of **Z1** and **T*n*** ($n = 2, 3, 6, 8$) have been measured using the Z-scan method at the 1064-nm wavelength.[56] In contrast to the case of **Y*n***, the incident laser is already one-photon resonant with the Q_x band (1068 nm) of **T2**, and the γ values of **T*n*** must derive from an interference of several one- and two-photon resonances with each detuning dependent on *n*. Therefore, an accurate estimation of the *n*-dependence of γ in a nonresonant condition is hampered, and we are hence forced to check the consistency of γ values only within theories. Because of the basis-set dependence of γ values similar to the case of **Y*n***, the **T2**/**Z1** γ_s ratio is reduced from 118 at the HF/6-31G* level to 21 at the HF/6-31G*+p level. In comparison with the latter, the corresponding ratio of 45 at the PPP level is much greater, which could be mainly ascribed to an underestimation for **Z1** based on the enhancement factor of γ_s proceeding from the HF/6-31G*+p to the PPP levels: **Z1** (1.4), **T2** (3.1), **Y1** (3.1), and **Y2** (3.6).

The results of the B3LYP calculations are also shown in Tables 2 and 3. The **Y2**/**Y1** γ_s ratios of 217 obtained with the

6-31G* basis set and even 112 at the 6-31G*+p level are much larger than the corresponding values of PPP and ab initio HF calculations as well as the experiments. This could be ascribed to the well-known feature of conventional DFT, i.e., an overestimation of the *n*-dependence of γ as pointed out on *trans*-**PA**[57] and diphenylacetylene.[58] However, it seems that the B3LYP method can be successfully applied to the multiply linked dimers, **D2** and **T2**, as well as the fused dimer, **B2**. Since the drawback of the DFT becomes more significant as the bond-length alternation is increased in *trans*-**PA**,[57] it is noteworthy that both diphenylacetylene and **Y2** comprise strongly alternated single linkage (−C≡C−), whereas the other diporphyrins contain no such fragments.

On the basis of the above considerations, the variation in γ values among diporphyrins can be correctly described even without diffuse basis functions, i.e., at the 6-31G* level. The relative γ_s values of diporphyrins with respect to **T2** are also shown in Table 2. It can be seen that the ab initio HF and the B3LYP theories provide similar results except for the failure of the latter on **Y2**, and the PPP theory is also consistent with these high-level theories except the relatively small γ of **Z2** and **B2**. It seems that the indirect interporphyrinic π-conjugation of **Z2**[59] would be underestimated by the present PPP parametrization. The discrepancy on **B2** is not due to the simplified molecular geometry adopted in the PPP calculations but is intrinsic to the PPP approximation, because essentially the same results were obtained even if the B3LYP/6-31G* optimized geometries were adopted. However, apart from this, we expect that the PPP theory will properly describe the structure−property relationship for γ in longer porphyrin arrays.

It is also noteworthy that the variation in γ values among diporphyrins cannot be interpreted on the basis of the HOMO−LUMO energy gap (E_g), because γ_s of **T2**, which has the smallest E_g, is reduced from those of **D2** and **Y2** (Table 2). In this regard, we note from the HF/6-31G* calculations that, although γ_{xxxx} is the dominant γ tensor component in these systems, **T2** has a relatively large and positive γ_{xxyy} value as in the case of **Z1**. This suggests a somewhat two-dimensional nature in the π-conjugation of **T2** which tends to reduce γ relative to the one-dimensional system.[25] Nevertheless, it will be shown that **T*n*** exhibits a much more remarkable evolution of γ/n than the other porphyrin arrays along with an increase in the number of porphyrin moieties.

Nonlinear Optical Properties of Porphyrin Arrays. For the longer porphyrin arrays ($n \geq 3$), we focus on the longitudinal components of α (α_{xx}) and γ (γ_{xxxx}), because they are the dominant components for quasi one-dimensional π-conjugated systems including the porphyrin arrays under study. We find that **T*n*** exhibits a dramatic evolution of γ_{xxxx}/n along with increasing *n*. For instance, the γ_{xxxx}/n values of **Y10**, **T10**, **D10**, and **B10** are calculated to be 2.05, 127, 15.0, and 1.23, respectively, in units of 10^{-32} esu (all of the calculated α_{xx} and γ_{xxxx} values are available in the Supporting Information). Because γ_s of these systems are dominated by the $\gamma_{xxxx}/5$ component (eq 10), γ_s/n of **T10** is enhanced by a factor of 23 200 with respect to the γ_s of **Z1**, which is 2 orders of magnitude greater than the corresponding ratio of 124 in proceeding from **Y1** to **Y10**.

The *n*-dependence of both α_{xx}/n and γ_{xxxx}/n in the whole range of *n* is shown in Figure 6 for each porphyrin array. In the case of **Y*n*** (top panel), the γ_s/n values measured using the DFWM technique[48] are also plotted after being scaled by a common factor of 0.36 to coincide with the theoretical γ_{xxxx} ($\approx 5\gamma_s$) value at $n = 1$. Note that these data have been taken from experiments

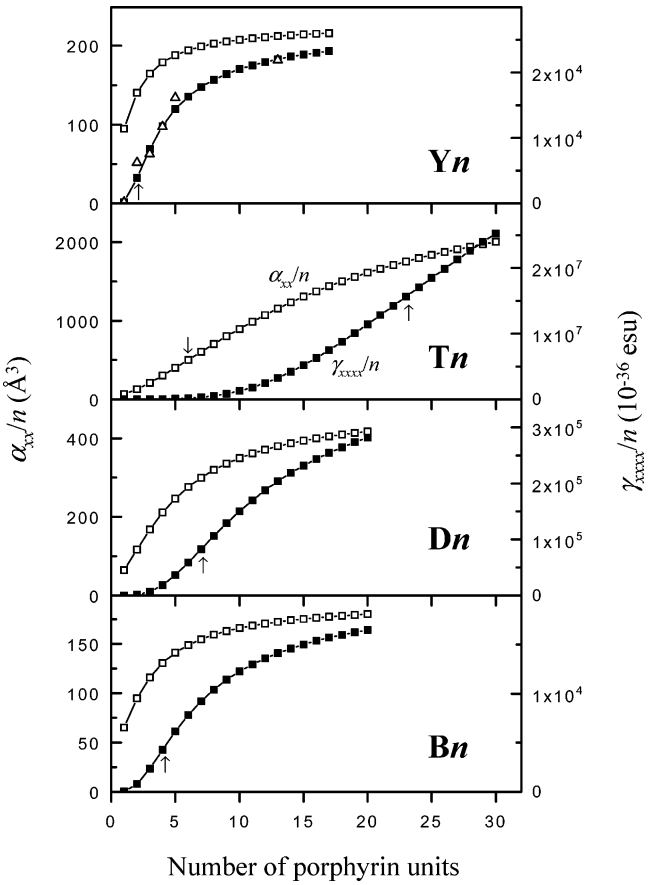

Figure 6. Dependence of α_{xx}/n and γ_{xxxx}/n values on the number of porphyrin units *n* of π-conjugated porphyrin arrays as obtained by the PPP−CPHF calculations. The experimental γ_s values of **Y*n*** taken from refs 48 and 14 are also plotted after being scaled by a factor of 0.36 (open triangle). The up and down arrows indicate the chain lengths at which γ_{xxxx}/n and α_{xx}/n turn into a saturation regime (see text).

on the commonly *meso*-aryl-substituted oligomers[48] and polymers (**1**·Quin$_n$ in ref 14), and the polymer length adopted in Figure 6 is an average of the estimated length of $n = 10-15$. As can be seen, the PPP calculation reproduces the observed *n*-dependence of γ_s/n for **Y*n*** quite well, and it predicts that the directly linked porphyrin arrays, **D*n*** and **T*n***, exhibit much more retarded saturation of both α_{xx}/n and γ_{xxxx}/n than **Y*n***, while a similar saturation behavior is the case of **B*n***.

As pointed out in the previous theoretical studies on *trans*-**PA**,[60,61] the saturation behavior of γ_{xxxx}/n can be characterized by the variation in its first derivative: $d[\gamma_{xxxx}/n]/dn$ successively increases until *n* reaches critical value N_γ, and after that, it starts decreasing to the thermodynamic limit, $d[\gamma_{xxxx}/n]/dn = 0$. This means that γ_{xxxx}/n turns into a saturation regime at $n = N_\gamma$, and we adopt N_γ as a measure of ECL. The N_γ values thus determined on various π-conjugated polymers are listed in Table 1 (constrained geometric unit). We find that L_γ (L_x of the N_γ-mer) of **Y*n*** is close to that of *trans*-**PA**, while those of **D*n*** and **T*n*** are increased two- and sevenfold, respectively. It is also noteworthy that N_γ is nearly identical to N_λ, which is determined from $\Delta\lambda_g$ of 32 nm (eq 12) in all the systems except **T*n***, thus implying the consistency of these ECLs. In sum-over-states (SOS) language,[62,63] the discrepancy on **T*n*** would be related to the fact that N_γ reflects the saturation of transition dipole moments associated with essential virtual transitions together with that of $1/E_g$ which determines N_λ. An exceptional feature of **T*n*** is also noted from the saturation behavior of α_{xx}/n:

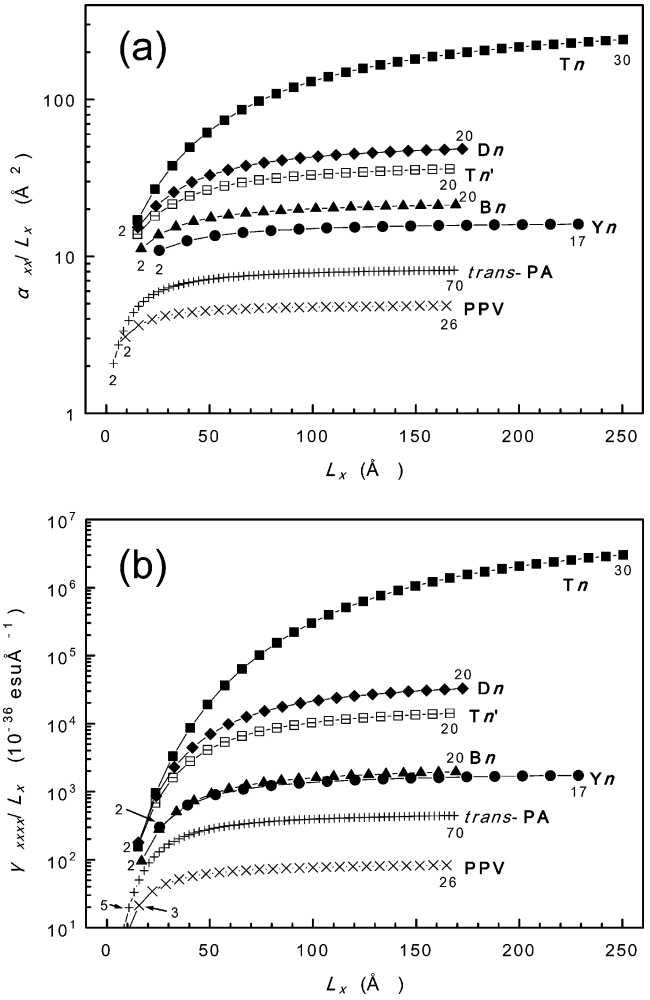

Figure 7. Dependence of (a) α_{xx}/L_x and (b) γ_{xxxx}/L_x values on chain length L_x of π-conjugated porphyrin arrays, *trans*-**PA**, and **PPV** as obtained by the PPP−CPHF calculations. The range of the number of repeating units n (Figure 1) is indicated.

$d[\alpha_{xx}/n]/dn$ reaching maximum at $n = 6$ for **T*n***, while α_{xx}/n is initially ($n = 2$) in the saturation regime for the other conjugated polymers.

The α_{xx} and γ_{xxxx} values of various π-conjugated oligomers normalized to their chain lengths L_x are plotted in Figure 7 to facilitate a comparison of macroscopic susceptibilities, $\chi^{(1)}$ and $\chi^{(3)}$, among different systems, while a consideration of chain density σ (the number of chains per unit cross-section) is also required. We note that the variation in γ_{xxxx}/L_x in these systems is quite similar to that of α_{xx}/L_x, implying the existence of a scaling relationship between these quantities. Because of this feature, we confine our attention to γ in the following discussion. The calculation predicts that $\chi^{(3)}$ of **Y*n*** polymer is comparable to that of *trans*-**PA**, taking into account a plausibly larger σ for the latter. Although the $\chi^{(3)}$ of **Y*n*** has been compared with those of other π-conjugated polymers based on the DFWM experiments,[13] a direct comparison of **Y*n*** and *trans*-**PA** was not permitted, because the measurement on the former was performed in the off-resonant condition, while the latter was at on-resonance. The comparison of off-resonant $\chi^{(3)}$ was made with **PDA** concluding that the $\chi^{(3)}$ of **Y*n*** is more than 10 times larger than that of **PDA**. As will be shown in Figures 9 and 10, the present calculations are consistent with this observation, even if a larger σ of **PDA** is taken into account.

Since all the porphyrin arrays are likely to have a similar σ, the variation in γ_{xxxx}/L_x among these systems may properly represent that in $\chi^{(3)}$. Then, it is predicted that even **D4** and **T4** oligomers exhibit larger $\chi^{(3)}$ than the **Y*n*** polymer, and the remarkable evolution of their $\chi^{(3)}$ values along with an increasing number of porphyrin moieties results in a 3 orders of magnitude enhancement by **T*n*** and a tenfold amplification by **D*n*** in the limit $n \rightarrow \infty$. According to recent experiments with femtosecond laser pulses, the TPA cross-section $\sigma^{(2)}$ of **T2** (14 000 GM)[18] exceeds that of **Y2** (9100 GM),[64] and from the present computational results on static γ, a much more dramatic enhancement of $\sigma^{(2)}$ is expected for longer **T*n***. In addition, it is evident from the comparison of **T*n*** and **T*n′*** that the remarkable NLO responses of **T*n*** are due to the cooperative contributions of the triple linkages as in the case of E_g.

For the application as all-optical signal processing, a material should fulfill the requirements of not only a sufficiently large NLO response but also transparency at the telecommunications windows near 1.3 and 1.5 μm. In comparison with the classical conjugated polymers such as **PDA**, the sharpness and high intensity of the Q-band absorption of **Y*n*** polymer around 850 nm should offer a stronger one-photon resonant enhancement of $\chi^{(3)}$ together with good transparency at the operating windows.[13] In this regard, **T*n*** will fall short of the transparency requirement, since its Q-band extends far into the red of the telecommunications window.[17b] Alternatively, **D*n*** may be promising for a further extension of the advantage of **Y*n***, because it also exhibits quite sharp, intense Q-band absorption that reaches approximately 1075 nm at $n = 5$,[20b] and the calculation predicts that even **D5** has larger $\chi^{(3)}$ than **Y*n*** polymer. Therefore, the measurements of $\chi^{(3)}(-\omega; \omega, \omega, -\omega)$ on **D*n*** at wavelengths within the telecommunications window would be particularly valuable.

Scaling Behaviors of $\chi^{(1)}$ and $\chi^{(3)}$. Using the Hückel theory, Flytzanis and co-workers have derived the scalings of $\chi^{(1)}$ and $\chi^{(3)}$ with a kind of ECL, delocalization parameter N_d or delocalization length L_d ($= N_d a$; a is the unit-cell length) (eqs 1 and 2).[23−25] For a simple bond-length alternated chain, N_d was defined as $N_d = (\beta_1 + \beta_2)/(\beta_1 - \beta_2)$ in terms of the modulated transfer integrals, β_1 (for C=C bonds) and β_2 (for C−C bonds). In the course of further study on these scaling laws, we adopt the above-mentioned N_γ as an ECL instead of N_d, because N_γ can be determined on an arbitrary π-conjugated polymer. The relationship between N_γ and N_d is examined at the PPP level on the basis of the same model chains as those of Flytzanis and co-workers. With the bond-length alternation parameter δ, the transfer integrals are represented by $\beta_1 = \beta_0(1 + \delta)$ and $\beta_2 = \beta_0(1 - \delta)$, which lead to a simple expression of the delocalization parameter, $N_d = 1/\delta$. The present β_1 and β_2 values used for *trans*-**PA** correspond to $\beta_0 = -2.338$ eV and $\delta = 0.084$. Other systems that have different ECLs are described by the same β_0 and variable δ, where the actual geometry required by the PPP theory is fixed in every case at that of standard *trans*-**PA** (i.e., bond-length alternated geometry). As pointed out in ref 65, **PDA** and σ-conjugated polysilane (**PS**) can be simulated by setting δ to 0.15 and ~0.3, respectively. The N_γ values of these systems are determined by the recipe described above and are compared with N_d ($= 1/\delta$) in Figure 8. As can be seen, N_γ is nearly proportional (accidentally identical) to N_d in the range of realistic δ ($1 \leq \delta \leq 0.08$), while the discrepancy becomes larger as δ decreases: in the limit $\delta \rightarrow 0$, $N_d \rightarrow \infty$ versus $N_\gamma = 21$. As stated below, this discrepancy is related to the occurrence of an off-diagonal charge density wave (CDW) as a Hartree−Fock solution of metallic *trans*-**PA**.

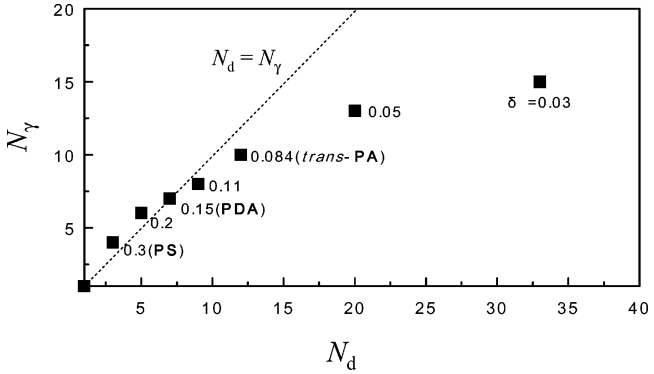

Figure 8. Relationship between effective conjugation lengths, N_d and N_γ (see text for the explanations), as evaluated using the PPP method on the simple conjugated chains of various bond-length alternation δ.

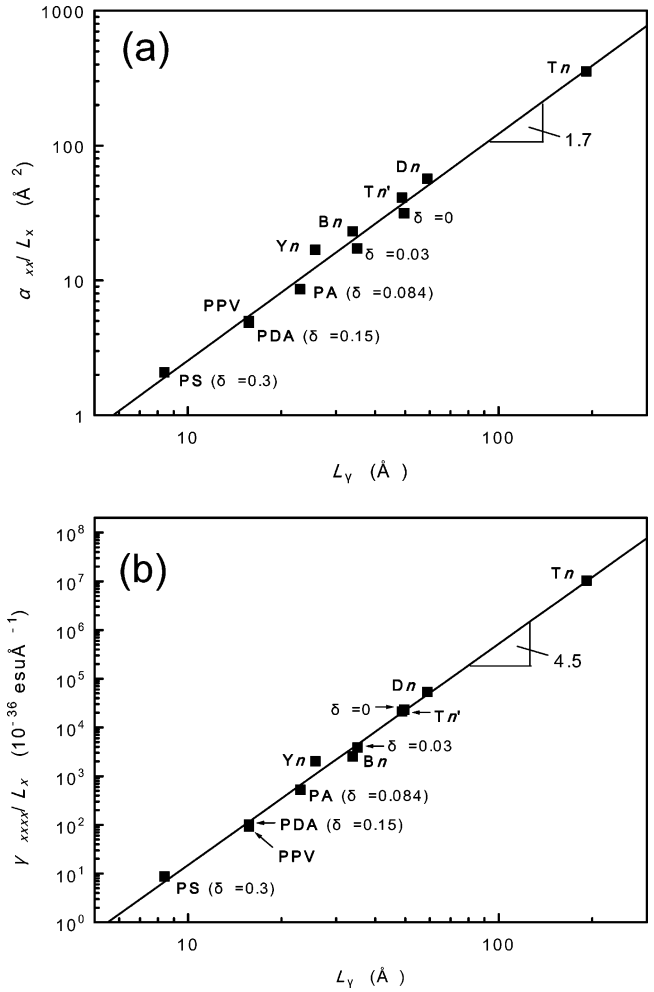

Figure 9. Double-logarithmic scale plot of PPP−CPHF calculated asymptotic values of (a) α_{xx}/L_x and (b) γ_{xxxx}/L_x vs effective conjugation length L_γ for various conjugated polymers. The fits to all the data points are shown by the solid lines with their slopes.

In the following, we are concerned with the α_{xx}/L_x and γ_{xxxx}/L_x values of infinitely long polymers, because the scaling relations (eqs 1−4) are valid for sufficiently long chains. Note that the variation of these quantities approximately represent those of $\chi^{(1)}$ and $\chi^{(3)}$. The asymptotic values of α_{xx}/L_x and γ_{xxxx}/L_x are estimated by extrapolating the finite-chain values via a fitting to the second-order polynomial of $1/L_x$ (see the Supporting Information). In Figure 9, they are plotted in a double-logarithmic scale versus L_γ (L_x of the N_γ-mer), where the simple model chains considered above (Figure 8) are indicated by each δ value. The least-squares linear fittings have been performed over all data points, and from the slope of these lines, we obtain the scaling laws, $\alpha_{xx}/L_x \sim L_\gamma^{1.7}$ and $\gamma_{xxxx}/L_x \sim L_\gamma^{4.5}$, which exhibit much smaller exponents than the Hückel values of 2 and 6. Because, due to the relationship between N_γ and N_d, our exponents should be further decreased if we adopt L_d instead of L_γ, these discrepancies are plausibly ascribed to the influence of electron−electron (e−e) interactions, which is taken into account in the PPP theory but not in the Hückel theory.

Although our results would be a better description of the scaling laws, any discussion concerning ECLs suffers from intrinsic difficulties. Because there is no unique definition for ECL, this is also the case for scaling relationships with respect to ECL. For instance, we obtain quite different power dependencies if we adopt L_E as an ECL, e.g., $\gamma_{xxxx}/L_x \sim L_E^{14.2}$ for the systems listed in Table 1. However, apart from these difficulties, the nice fittings in Figure 9 suggest that the asymptotic values of α_{xx}/L_x and γ_{xxxx}/L_x of any conjugated polymers could be estimated from these plots if we determine only their N_γ value. This offers apparent computational benefits, because N_γ can be determined with much less effort than a direct evaluation of the asymptotic values, especially for γ.

On the other hand, the scaling relationships of eqs 3 and 4 are well-defined and accessible to measurement. The experimental study has derived the scaling relationship of $\chi^{(3)}(-3\omega; \omega, \omega, \omega) \sim \lambda_{max}^x$ (λ_{max} is the wavelength of the low-energy absorption maximum) with the exponent $x = 11$ for various conjugated oligomers and polymers including *trans*- and *cis*-**PA** and **PPV**.[27] Another experiment has also obtained a similar value of $x = 10$ on a series of PPV derivatives with respect to the wavelength of the optical absorption edge.[26] In Figure 10, the asymptotic values of α_{xx}/L_x and γ_{xxxx}/L_x are plotted in a double-logarithmic scale versus reciprocal HOMO−LUMO energy gap $1/E_g$. From the linear fit to the five simple chains, we obtain the scaling relationships, $\alpha_{xx}/L_x \sim 1/E_g^{3.1}$ and $\gamma_{xxxx}/L_x \sim 1/E_g^{9.0}$, which can be compared with eqs 3 and 4 as well as with the experiments. These exponents are much larger than the Hückel values of 2 and 6, and that for γ is in much better agreement with the experimental results on $\chi^{(3)}$. Thus, taking into account e−e interactions indeed leads to an improved description of the scaling relationship. It is also noteworthy that the experimental λ_{max} is plausibly associated with an exciton, while the theoretical E_g corresponds to a free electron−hole state. The excitonic level is located below E_g by an exciton binding energy that tends to increase with an increasing δ.[66] Accordingly, if exciton formation is taken into account, the fitting lines in Figure 10 should be much steeper, and the exponent will hence be much closer to the experimental values.

At this stage, note that energy gap E_g of the simple conjugated chain does not vanish even at $\delta = 0$ (Figure 10), because the PPP−HF solution obtained for this system corresponds to the off-diagonal CDW.[67,68] The ab initio HF calculations have revealed that this solution is more stable than the metallic solution for the equidistant *trans*-**PA** and lies on the same potential energy surface as the asymmetric wave functions of bond-length alternated chains.[67] Because the occurrence of off-diagonal CDW within the HF model indicates a lattice dimerization of *trans*-**PA**[67,68] as explicitly described by Peierls distortion,[69] those systems with $\delta < 0.084$ are not realistic.

It has been pointed out that the scaling relationship of $\chi^{(3)} \sim \lambda_{max}^x$ obtained for a series of conjugated polymers does not hold in other systems that have different dimensionality of π-electron delocalization or substitution effects.[27] In other words, we can utilize the relevant masterplot ($\chi^{(3)}$ versus $1/E_g$ or λ_{max}) to

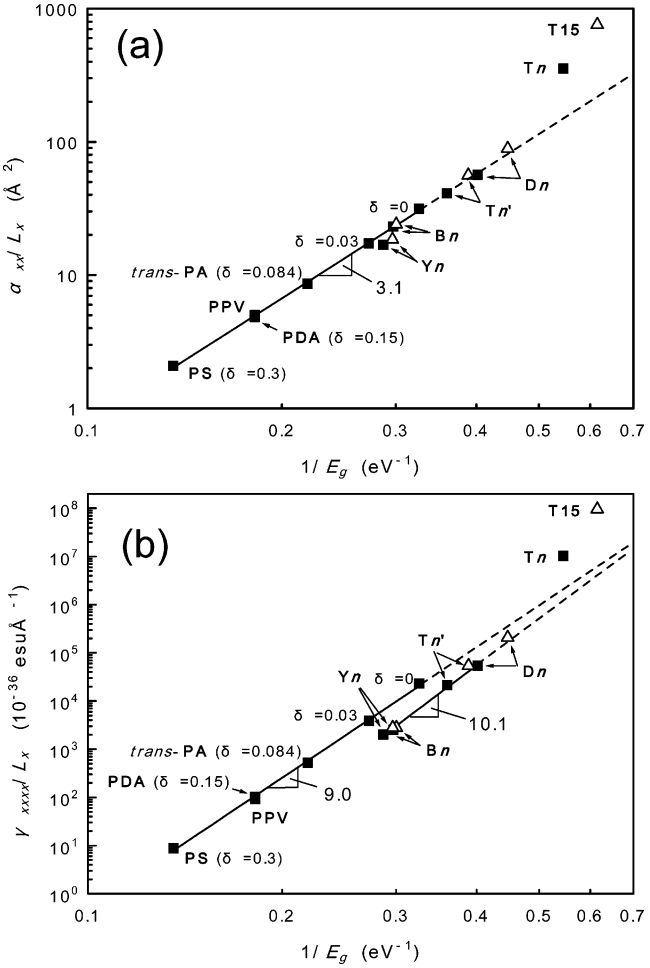

Figure 10. Double-logarithmic scale plot of PPP−CPHF calculated asymptotic values of (a) α_{xx}/L_x and (b) γ_{xxxx}/L_x vs reciprocal HOMO−LUMO energy gap $1/E_g$ for various conjugated polymers. The filled squares represent the data obtained for constrained geometries and the open triangles for relaxed geometries (note that γ_{xxxx} of **T15** has a negative sign). (a) The linear fit to the data of five simple chains is indicated. (b) The same fit as in (a) and another fit to the data of four porphyrin arrays (constrained geometries) are indicated.

characterize the electronic structures of new conjugated polymers such as porphyrin arrays in comparison with the typical one-dimensional polymers. As shown in Figure 10, α_{xx}/L_x of four porphyrin arrays (**Y*n***, **B*n***, **T*n′***, and **D*n***) are scaled together with the simple chains, and even their γ_{xxxx}/L_x values exhibit a scaling relationship (exponent is 10.1) similar to that of simple conjugated chains. These features would be a manifestation of typical one-dimensional π-conjugation of these porphyrin arrays. In SOS language, the amount of charge separation associated with virtual electronic transitions is a crucial quantity that determines the magnitude of corresponding transition dipole moments and hence, those of α and γ.[62,63] Therefore, the slightly reduced γ of these porphyrin arrays relative to the simple chains can be attributed to a less significant charge separation associated with virtual transitions between excited states, because their α values are essentially of the same magnitude as the simple conjugated chains.

On the other hand, the large γ value of **T*n*** cannot be expected from those of the other porphyrin arrays along their scaling behavior and is even beyond the extrapolation from the simple conjugated chains. This feature is due to the extremely retarded saturation of γ_{xxxx}/L_x relative to $1/E_g$ compared with the other porphyrin arrays as has already been recognized from the comparison of two kinds of ECL: N_γ is much greater than N_λ ($\Delta\lambda = 32$ nm) for **T*n***, while they are essentially the same in the other conjugated polymers (Table 1). Because there is also a similar situation in the case of α (Figure 10a), the exceptionally large γ of **T*n*** would result mainly from the significant charge separation associated with the ground to the excited Q_x state transition as revealed in our previous study.[43] Thus, **T*n*** can be viewed as indeed a new type of π-conjugated polymer in the masterplots due to an extremely extended π-conjugation that is established by the triple linkage of porphyrin moieties.

Influence of Geometry Relaxation of Porphyrin Units. In all of the PPP calculations described above, the geometries of the porphyrin units in the arrays were constrained to the X-ray geometry of Zn^{II}-TPP. Therefore, it is worthwhile to consider how their relaxation affects the ECLs and, hence, the NLO properties of porphyrin arrays. For this purpose, we optimized the geometry of porphyrin trimers using the B3LYP/6-31G* method and adopted the bond lengths in their central units to evaluate all of the intraunit transfer integrals in the PPP Hamiltonian. Note that the geometry relaxations are taken into account by changing only these transfer integrals in the previous models (i.e., e−e interactions are not changed), because they must be the most essential parameters in describing the electronic structures of π-conjugated systems.

The ECLs of porphyrin arrays after geometry relaxations are summarized in the bottom of Table 1. The ECLs of **Y*n*** and **B*n*** are almost same as those for the constrained geometries, while those of **D*n*** are slightly increased and N_λ ($\Delta\lambda_g = 32$ nm) of **T*n*** is dramatically enhanced. Although N_γ could not be determined for **T*n*** of relaxed geometries because of convergence problems of CPHF calculations for $n \geq 16$, it is evident from the n-dependence of γ_{xxxx}/n described below that N_γ is also significantly increased. The asymptotic values of α_{xx}/L_x (γ_{xxxx}/L_x) for the relaxed geometries were estimated for the porphyrin arrays except **T*n*** using the same procedure as described above, and it was found that they are increased by factors of 1.1 (1.4), 1.0 (1.1), 1.4 (2.6), and 1.6 (3.9) for **Y*n***, **B*n***, **T*n′***, and **D*n***, respectively.

For **T*n***, the α_{xx}/n and γ_{xxxx}/n values of the relaxed geometries are compared with those of the constrained geometries in Figure 11a,b, respectively. As a result of geometry relaxations, α_{xx}/n is increased by factors of 2.2 and 4.8 at $n = 10$ and 15, respectively, and it does not indicate any saturation even at $n = 15$. The change in γ is more drastic; γ_{xxxx} becomes negative at $n = 7$, and it is enhanced by factors of −4.3 and −153 at $n = 10$ and 15, respectively, relative to those of the constrained geometries. It is noteworthy that these dramatic changes are attributed largely to the triple linkage, because only slight changes are the case for **T*n′***, which has the same unit geometries as **T*n*** but only *meso*−*meso* linkage. In comparison with the X-ray structure of Zn^{II}-TPP as well as the B3LYP/6-31G* optimized structure of Zn^{II}-porphin (**Z1**), we note that both the $C_{meso}-C_\alpha$ and $C_\beta-C_\beta$ bonds next to the interunit linkages are significantly elongated in the central unit of **T3** (the same trend of the $C_{meso}-C_\alpha$ bond is also the case for quinoidal porphyrin[70]). These geometrical features may be responsible for a further enhancement of charge separation in the excited Q_x state (i.e., an increase in α) and, hence, for the negative sign of γ via a dominant contribution from the negative term of SOS expression of γ (the second term of eq 30 in ref 5).

The data for the relaxed geometries are also plotted in the masterplots of Figure 10. As can be seen, the geometry relaxation of porphyrin units does not alter the trends of the structure−property relationships among porphyrin arrays; rather, it makes the unique features of **T*n*** more prominent under the

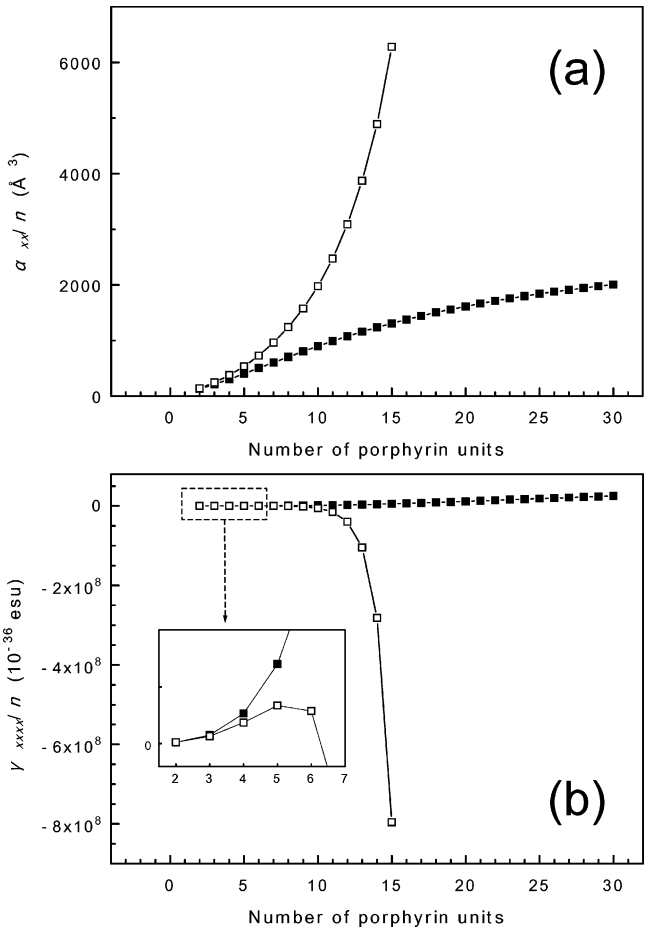

Figure 11. Influence of geometrical relaxations of porphyrin units on the *n*-dependence of (a) α_{xx}/n and (b) γ_{xxxx}/n of **T*n*** as obtained by the PPP−CPHF calculations (■, constrained geometry; □, relaxed geometry; inset expanded in (b)).

present considerations. Although the significant geometry dependence of γ may indicate an interesting development in the material design based on **T*n***, it is of primary importance to predict more precisely the NLO properties of **T*n***, especially the sign and *n*-dependence of γ/n for the relatively short oligomers ($n \leq 10$), using more sophisticated computational models.

IV. Conclusions

The second hyperpolarizabilities (γ) of various π-conjugated porphyrin arrays and classical conjugated polymers have been calculated using the PPP−CPHF method. The accuracy of the PPP theory has been confirmed by the calculations at the ab initio HF and B3LYP levels of theory in the case of porphyrin monomers and dimers. We found that the *meso*−β doubly linked porphyrin array **D*n*** and especially the *meso*−*meso*, $\beta-\beta$, $\beta-\beta$ triply linked array **T*n*** exhibit much more remarkable evolution of γ/n with an increase in the number of porphyrin units *n* than the butadiyne-bridged array **Y*n***. As a result, static third-order susceptibilities $\chi^{(3)}$ of **D*n*** and **T*n*** are predicted to be larger than that of **Y*n*** by 1 and 3 orders of magnitude, respectively, in the limit $n \rightarrow \infty$, and these advantages of porphyrin tapes become more prominent by taking into account geometrical relaxations of the porphyrin units in the arrays. On the basis of these results, both **D*n*** and **T*n*** are promising candidates for a further improvement in NLO responses such as two-photon absorption, while for applications that require transparency at the operating window, **D*n*** would be more favorable.

As a measure of effective conjugation length (ECL), we propose oligomer length L_γ at which γ/n turns into a saturation regime. It was found that L_γ of **Y*n*** is similar to that of *trans*-**PA**, while those of **D*n*** and **T*n*** are increased two- and sevenfold, respectively, and further enhancements are caused by geometrical relaxations, especially for **T*n***. Both $\chi^{(1)}$ and $\chi^{(3)}$ of various conjugated polymers are systematically described by L_γ, in which the power dependencies are much lower than the results of the Hückel theory (eqs 1 and 2) because of the influence of electron−electron (e−e) interactions. In addition, eqs 3 and 4 were reinvestigated for a series of simple conjugated chains. Especially for the relationship, $\chi^{(3)} \sim 1/E_g^x$, the PPP theory provides the exponent of $x = 9.0$, which is in much better agreement with the experiments ($x = 10-11$) than the Hückel theory ($x = 6$), revealing a significant role of e−e interactions on this issue.

The porphyrin arrays except **T*n*** exhibit a similar scaling relationship ($x = 10.1$) consistent with the quasi one-dimensional nature of these π-systems. However, the extremely large γ value of **T*n*** cannot be expected from those of the other porphyrin arrays or the simple conjugated chains along the scaling behavior of ordinary one-dimensional π-systems. In this sense, **T*n*** is regarded as indeed a new type of π-conjugated polymer probably due to extremely delocalized π-electrons along the tape-shaped backbone. Thus, a similar analysis based on the master plot of $\chi^{(3)}$ versus $1/E_g$ (or the λ_{max} of optical absorption) would be useful for a systematic understanding of the structure−property relationship among various quasi one-dimensional conjugated polymers. In addition, from the remarkable advantage of the triple linkage of **T*n***, a question arises as to whether the same architecture is effective for π-conjugation if other macrocycles, such as corroles[71] and N-confused porphyrins,[72] are adopted as building block elements.

Acknowledgment. A.O. acknowledges support by Grant-in-Aids for Scientific Research (nos. 12874076, 12440196, and 11223205) from the Ministry of Education, Science, Sports and Culture of Japan, and by CREST (Core Research for Evolutional Science and Technology) of the Japan Science and Technology Corporation (JST). K.T. acknowledges support by a Grant-in-Aid for Scientific Research (no. 16350100) from the Ministry of Education, Science, Sports and Culture of Japan, and by CREST (Core Research for Evolutional Science and Technology) of the Japan Science and Technology Corporation (JST).

Supporting Information Available: Tables S1−S11 contain all the data from the PPP calculations: HOMO and LUMO energies, HOMO−LUMO energy gap, and α_{xx} and γ_{xxxx} values. This material is available free of charge via the Internet at http://pubs.acs.org.

References and Notes

(1) *Nonlinear Optical Properties of Organic and Polymeric Materials*; Williams, D. J., Ed.; ACS Symposium Series 233; American Chemical Society: Washington, DC, 1984.

(2) *Nonlinear Optical Properties of Organic Molecules and Crystals*; Chemla, D. S., Zyss, J., Eds.; Academic Press: Orlando, 1987; Vols. 1 and 2.

(3) *Nonlinear Optical Properties of Polymers*; Heeger, A. J., Orenstein, J., Ulrich, D. R., Eds.; Materials Research Society Symposium Proceedings; Materials Research Society: Pittsburgh, 1988; Vol. 109.

(4) Prasad, P. N.; Williams, D. J. *Introduction to Nonlinear Optical Effects in Molecules and Polymers*; Wiley: New York, 1991.

(5) Brédas, J. L.; Adant, C.; Tackx, P.; Persoons, A. *Chem. Rev.* **1994**, *94*, 243.

(6) Halvorson, C.; Hays, A.; Kraabel, B.; Wu, R.; Wudl, F.; Heeger, A. J. *Science* **1994**, *265*, 1215.

(7) Parthenopoulos, D. A.; Rentzepis, P. M. *Science* **1989**, *245*, 843.

(8) Ehrlich, J. E.; Wu, X. L.; Lee, I.-Y. S.; Hu, Z.-Y.; Röckel, H.; Marder, S. R.; Perry, J. W. *Opt. Lett.* **1997**, *22*, 1843.

(9) Bhawalkar, J. D.; Kumar, N. D.; Zhao, C. F.; Prasad, P. N. *J. Clin. Laser Med. Surg.* **1997**, *15*, 201.
(10) Carter, G. M.; Chen, Y. J.; Rubner, M. F.; Sandman, D. J.; Thakur, M. K.; Tripathy, S. K. In *Nonlinear Optical Properties of Organic Molecules and Crystals*; Chemla, D. S., Zyss, J., Eds.; Academic Press: Orlando, 1987; Vol. 2, p 85.
(11) Singh, B. P.; Prasad, P. N.; Karasz, F. E. *Polymer* **1988**, *29*, 1940.
(12) (a) Anderson, H. L.; Martin, S. J.; Bradley, D. D. C. *Angew. Chem., Int. Ed. Engl.* **1994**, *33*, 655. (b) Anderson, H. L. *Chem. Commun.* **1999**, 2323.
(13) Kuebler, S. M.; Denning, R. G.; Anderson, H. L. *J. Am. Chem. Soc.* **2000**, *122*, 339.
(14) Screen, T. E. O.; Thorne, J. R. G.; Denning, R. G.; Bucknall, D. G.; Anderson, H. L. *J. Am. Chem. Soc.* **2002**, *124*, 9712.
(15) Aratani, N.; Osuka, A.; Kim, Y. H.; Jeong, D. H.; Kim, D. *Angew. Chem., Int. Ed.* **2000**, *39*, 1458.
(16) (a) Ohta, N.; Iwaki, Y.; Ito, T.; Yamazaki, I.; Osuka, A. *J. Phys. Chem. B* **1999**, *103*, 11242. (b) Matsuzaki, Y.; Nogami, A.; Iwaki, Y.; Ohta, N.; Yoshida, N.; Aratani, N.; Osuka, A.; Tanaka, K. *J. Phys. Chem. A* **2005**, *109*, 703.
(17) (a) Tsuda, A.; Furuta, H.; Osuka, A. *Angew. Chem., Int. Ed.* **2000**, *39*, 2549. (b) Tsuda, A.; Osuka, A. *Science* **2001**, *293*, 79.
(18) Kim, D. Y.; Ahn, T. K.; Kwon, J. H.; Kim, D.; Ikeue, T.; Aratani, N.; Osuka, A.; Shigeiwa, M.; Maeda, S. *J. Phys. Chem. A* **2005**, *109*, 2996.
(19) Inokuma, Y.; Ono, N.; Uno, H.; Kim, D. Y.; Noh, S. B.; Kim, D.; Osuka, A. *Chem. Commun.* **2005**, 3782.
(20) (a) Tsuda, A.; Nakano, A.; Furuta, H.; Yamochi, H.; Osuka, A. *Angew. Chem., Int. Ed.* **2000**, *39*, 558. (b) Tsuda, A.; Nakamura, Y.; Osuka, A. *Chem. Commun.* **2003**, 1096.
(21) (a) Jaquinod, L.; Siri, O.; Khoury, R. G.; Smith, K. M. *Chem. Commun.* **1998**, 1261. (b) Paolesse, R.; Jaquinod, L.; Sala, F. D.; Nurco, D. J.; Prodi, L.; Montalti, M.; Natale, C. D.; D'Amico, A.; Carlo, A. D.; Lugli, P.; Smith, K. M. *J. Am. Chem. Soc.* **2000**, *122*, 11295.
(22) Martin, R. E.; Diederich, F. *Angew. Chem., Int. Ed.* **1999**, *38*, 1351.
(23) Cojan, C.; Agrawal, G. P.; Flytzanis, C. *Phys. Rev. B* **1977**, *15*, 909.
(24) Agrawal, G. P.; Cojan, C.; Flytzanis, C. *Phys. Rev. B* **1978**, *17*, 776.
(25) Flytzanis, C. In *Nonlinear Optical Properties of Organic Molecules and Crystals*; Chemla, D. S., Zyss, J., Eds.; Academic Press: Orlando, 1987; Vol. 2, p 121.
(26) Kanbara, H.; Kobayashi, H.; Kaino, T.; Ooba, N.; Kurihara, T. *J. Phys. Chem.* **1994**, *98*, 12270.
(27) Mathy, A.; Ueberhofen, K.; Schenk, R.; Gregorius, H.; Garay, R.; Müllen, K.; Bubeck, C. *Phys. Rev. B* **1996**, *53*, 4367.
(28) Pariser, R.; Parr, R. G. *J. Chem. Phys.* **1953**, *21*, 767.
(29) Pople, J. A. *Trans. Faraday Soc.* **1953**, *42*, 1375.
(30) Frisch, M. J.; Trucks, G. W.; Schlegel, H. B.; Scuseria, G. E.; Robb, M. A.; Cheeseman, J. R.; Zakrzewski, V. G.; Montgomery, J. A.; Stratmann, R. E.; Burant, J. C.; Dapprich, S.; Millam, J. M.; Daniels, A. D.; Kudin, K. N.; Strain, M. C.; Farkas, O.; Tomasi, J.; Barone, V.; Cossi, M.; Cammi, R.; Mennucci, B.; Pomelli, C.; Adamo, C.; Clifford, S.; Ochterski, J.; Petersson, G. A.; Ayala, P. Y.; Cui, Q.; Morokuma, K.; Malick, D. K.; Rabuck, A. D.; Raghavachari, K.; Foresman, J. B.; Cioslowski, J.; Ortiz, J. V.; Baboul, A. G.; Stefanov, B. B.; Liu, G.; Liashenko, A.; Piskorz, P.; Komaromi, I.; Gomperts, R.; Martin, R. L.; Fox, D. J.; Keith, T.; Al-Laham, M. A.; Peng, C. Y.; Nanayakkara, A.; Gonzalez, C.; Challacombe, M.; Gill, P. M. W.; Johnson, B.; Chen, W.; Wong, M. W.; Andres, J. L.; Gonzalez, C.; Head-Gordon, M.; Replogle, E. S.; Pople, J. A. *Gaussian 98*, revision, A.7; Gaussian, Inc.: Pittsburgh, PA, 1998.
(31) Sekino, H.; Kobayashi, H. *J. Chem. Phys.* **1987**, *86*, 5045.
(32) Taylor, P. N.; Huuskonen, J.; Rumbles, G.; Aplin, R. T.; Williams, E.; Anderson, H. L. *Chem. Commun.* **1998**, 909.
(33) Weiss, C.; Kobayashi, H.; Gouterman, M. *J. Mol. Spectrosc.* **1965**, *16*, 415.
(34) Nishimoto, K.; Mataga, N. *Z. Phys. Chem.* **1957**, *12*, 335.
(35) See, for instance, Dykstra, C. E.; Jasien, P. G. *Chem. Phys. Lett.* **1984**, *109*, 388.
(36) Hehre, W. J.; Ditchfield, R.; Pople, J. A. *J. Chem. Phys.* **1972**, *56*, 2257.
(37) Hariharan, P. C.; Pople, J. A. *Theor. Chim. Acta* **1973**, *28*, 213.
(38) Huzinaga, S.; Andzelm, J.; Klobukowski, M.; Radzio-Andzelm, E.; Sakai, Y.; Tatewaki, H. *Gaussian Basis Sets for Molecular Calculations*; Elsevier: New York, 1984.
(39) Schmidt, M. W.; Baldridge, K. K.; Boatz, J. A.; Elbert, S. T.; Gordon, M. S.; Jensen, J. H.; Koseki, S.; Matsunaga, N.; Nguyen, K. A.; Su, S.; Windus, T. L.; Dupuis, M.; Montgomery, J. A. *J. Comput. Chem.* **1993**, *14*, 1347.
(40) Gouterman, M. *J. Chem. Phys.* **1959**, *30*, 1139.
(41) Tsuda, A.; Furuta, H.; Osuka, A. *J. Am. Chem. Soc.* **2001**, *123*, 10304.
(42) Bonifazi, D.; Scholl, M.; Song, F.; Echegoyen, L.; Accorsi, G.; Armaroli, N.; Diederich, F. *Angew. Chem., Int. Ed.* **2003**, *42*, 4966.
(43) Cho, H. S.; Jeong, D. H.; Cho, S.; Kim, D.; Matsuzaki, Y.; Tanaka, K.; Tsuda, A.; Osuka, A. *J. Am. Chem. Soc.* **2002**, *124*, 14642.
(44) Yamaguchi, Y. *J. Chem. Phys.* **2002**, *117*, 9688.
(45) Miyahara, T.; Nakatsuji, H.; Hasegawa, J.; Osuka, A.; Aratani, N.; Tsuda, A. *J. Chem. Phys.* **2002**, *117*, 11196.
(46) Spellane, P. J.; Gouterman, M.; Antipas, A.; Kim, S.; Liu, Y. C. *Inorg. Chem.* **1980**, *19*, 386.
(47) Vangberg, T.; Lie, R.; Ghosh, A. *J. Am. Chem. Soc.* **2002**, *124*, 8122.
(48) Thorne, J. R. G.; Kuebler, S. M.; Denning, R. G.; Blake, I. M.; Taylor, P. N.; Anderson, H. L. *Chem. Phys.* **1999**, *248*, 181.
(49) (a) André, J. M.; Gouverneur, L.; Leroy, G. *Int. J. Quantum Chem.* **1967**, *1*, 427. (b) André, J. M.; Gouverneur, L.; Leroy, G. *Int. J. Quantum Chem.* **1967**, *1*, 451.
(50) Del Re, G.; Ladik, J.; Biczó, G. *Phys. Rev.* **1967**, *155*, 997.
(51) Suhai, S. *Phys. Rev. B* **1983**, *27*, 3506.
(52) Meier, H.; Stalmach, U.; Kolshorn, H. *Acta Polym.* **1997**, *48*, 379.
(53) Matsuzawa, N.; Ata, M.; Dixon, D. A. *J. Phys. Chem.* **1995**, *99*, 7698.
(54) Yamada, S.; Nakano, M.; Shigemoto, I.; Yamaguchi, K. *Chem. Phys. Lett.* **1996**, *254*, 158.
(55) Hurst, G. J. B.; Dupuis, M.; Clementi, E. *J. Chem. Phys.* **1988**, *89*, 385.
(56) Kim, D.; Osuka, A. *J. Phys. Chem. A* **2003**, *107*, 8791.
(57) Champagne, B.; Perpète, E. A.; van Gisbergen, S. J. A.; Baerends, E. J.; Snijders, J. G.; Soubra-Ghaoui, C.; Robins, K. A.; Kirtman, B. *J. Chem. Phys.* **1998**, *109*, 10489.
(58) Nakano, M.; Fujita, H.; Takahata, M.; Yamaguchi, K. *J. Am. Chem. Soc.* **2002**, *124*, 9648.
(59) Yoshida, N.; Ishizuka, T.; Osuka, A.; Jeong, D. H.; Cho, H. S.; Kim, D.; Matsuzaki, Y.; Tanaka, K.; Nogami, A.; Tanaka, K. *Chem.—Eur. J.* **2003**, *9*, 58.
(60) Mukamel, S.; Takahashi, A.; Wang, H. X.; Chen, G. *Science* **1994**, *266*, 250.
(61) Kirtman, B.; Toto, J. L.; Robins, K. A.; Hasan, M. *J. Chem. Phys.* **1995**, *102*, 5350.
(62) Heflin, J. R.; Wong, K. Y.; Zamani-Khamiri, O.; Garito, A. F. *Phys. Rev. B* **1988**, *38*, 1573.
(63) Pierce, B. M. *J. Chem. Phys.* **1989**, *91*, 791.
(64) Drobizhev, M.; Stepanenko, Y.; Dzenis, Y.; Karotki, A.; Rebane, A.; Taylor, P. N.; Anderson, H. L. *J. Am. Chem. Soc.* **2004**, *126*, 15352.
(65) McWilliams, P. C. M.; Hayden, G. W.; Soos, Z. G. *Phys. Rev. B* **1991**, *43*, 9777.
(66) Gallagher, F. B.; Mazumdar, S. *Phys. Rev. B* **1997**, *56*, 15025.
(67) Kertész, M.; Koller, J.; Ažman, A. *Int. J. Quantum Chem.* **1980**, *18*, 645.
(68) Tanaka, K.; Kobayashi, H.; Yamanaka, S.; Yoshizawa, K.; Yamabe, T. *J. Chem. Phys.* **1989**, *91*, 3724.
(69) Peierls, R. E. *Quantum Theory of Solids*; Clarendon: Oxford, 1955.
(70) Blake, I. M.; Anderson, H. L.; Beljonne, D.; Brédas, J. L.; Clegg, W. *J. Am. Chem. Soc.* **1998**, *120*, 10764.
(71) Johnson, A. W.; Kay, I. T. *Proc. Chem. Soc.* **1964**, 89.
(72) (a) Furuta, H.; Asano, T.; Ogawa, T. *J. Am. Chem. Soc.* **1994**, *116*, 767. (b) Chmielewski, P. J.; Latos-Grażyński, L.; Rachlewicz, K.; Glowiak, T. *Angew. Chem., Int. Ed. Engl.* **1994**, *33*, 779.